Magnetic Resonance Imaging, Vol. 16, Nos. 5/6, pp. 451–454, 1998

Printed in the USA.
0730-725X/98 $19.00 + .00

PII S0730-725X(98)00073-3

● *Invited Lecture*

FLUID FLOW IN POROUS SYSTEMS

P. MANSFIELD AND M. BENCSIK

Magnetic Resonance Centre, Department of Physics, University of Nottingham, Nottingham, UK

Nuclear magnetic resonance (NMR) measurements of water velocity flowing through glass bead packs with a bead diameter of 10 mm have been made using the π echo-planar imaging (PEPI) sequence. These results indicate that for various flow rates the flow variance is proportional to the mean flow velocity in agreement with the Mansfield-Issa equation. The velocity distributions are approximately Gaussian. Investigation of the slopes of the variance vs. velocity curves as a function of slice thickness indicate some coherence effects in the connectivity of the glass bead system. An extension of an earlier intervoxel coupling model is presented, which seems to explain the observed coherence effects. © 1998 Elsevier Science Inc.

Keywords: **Fluid transport; PEPI; Glass bead phantoms.**

INTRODUCTION

The π echo-planar imaging (PEPI) method of flow imaging[1] has recently been applied successfully to measure fluid flow and in particular the velocity distribution across a transaxial slice in Bentheimer and Clashach sandstone, and more recently in glass bead phantoms. In all cases the velocity distributions obtained are characterised by an approximate Gaussian distribution curve and a velocity variance proportional to mean flow velocity, which agrees with theoretical predictions based on a stochastic model of flow.[2]

In a microscopic model of flow a complementary description of the coupling process between adjacent pixels is used to evaluate the velocity variance. This model also leads to the velocity variance being proportional to mean flow velocity, i.e., the Mansfield–Issa equation.[3] In all flow velocity distributions the mean velocity of course obeys Darcy's Law.

The change in variance with mean flow velocity has been attributed to the presence of transverse flow orthogonal to the main flow pressure gradient. This transverse flow has been ascribed to an intervoxel coupling mechanism comprising Bernoulli flow channels, which allow non-dissipative transverse flow across the slice. Using this model, the coupling mechanism is further investigated for an isolated voxel pair. It is shown that the characteristic way in which the fluid velocity in a particular voxel changes with slice thickness depends on the dimensions of the voxel.

THEORETICAL BACKGROUND

We have shown elsewhere[3] that, for a set of isolated pairs of voxels of cross-sectional area dA each with a single nondissipative flow channel or Bernoulli pathway of cross-sectional area Δa_j forming the coupling path for fluid transfer between voxels, the velocity variance calculated for all pairs is given by:

$$a^2 = k \sum_j \left(\frac{\Delta a_j}{dA}\right) \left(\frac{\Delta k_j}{k}\right) \bar{v}/\rho N = k \frac{\bar{v}}{\rho N} \sum_j C_j, \quad (1)$$

where $\bar{v}$ is the mean flow velocity, N is the number of voxels in the slice, k is the sample resistivity, ρ the fluid density, Δk_j a small resistive element, and where the subscript j is used to tag the characteristics of the j^{th} voxel.

For this approximation to hold, we require $(\Delta a_j/dA)^2 < 1$, a situation which obtains naturally in the real system, because the in-plane resolution is 1.9 mm per pixel and the pore diameter is of the order of 20 μm.

Taking $\Delta a_j = \Delta a$, Eq. (1) leads to the Mansfield-Issa equation, where from Eqs. (1) and (2) the connectivity, $\langle C \rangle$, is given by:

Address correspondence to Sir Peter Mansfield, FRS, University Park, Nottingham NG7 2RD, UK.

$$\langle C\rangle = \frac{1}{N}\sum_j C_j = \sum_j \left(\frac{\Delta a}{dA}\right)^2 \left(\frac{\Delta k_j}{k}\right)/N. \qquad (2)$$

The Gaussian velocity distribution derived previously[2] is expressed as a percentage of the number n of voxels with flow velocity v to the total number of voxels, N, and is given by:

$$n/N = \frac{[100\delta v]}{a\sqrt{2\pi}} \exp[-(v-\bar{v})^2/2a^2], \qquad (3)$$

where δv is the flow interval used in plotting the histogram data.

Extension of Model

In a straightforward extension of the above voxel coupling model, we introduce m additional coupling pathways. For a single pathway we have shown previously[3] that the spatial correlation function, $f(z)$, describing the intervoxel connectivity is given by:

$$f(z) = e^{-|z|/\lambda}, \qquad (4)$$

where λ is the mean misregistration length of entry and exit orifices measured along the z-axis.

The normalised distribution of $N/2$ voxel pairs, each having a single connecting Bernoulli flow channel with entry and exit orifices displaced by z, is from the above discussion equal to:

$$F(z) = \tfrac{1}{2}\frac{N}{\lambda} e^{-|z|/\lambda}. \qquad (5)$$

In modeling the single coupling channel, we used a resistive network, two arms of which correspond to dissipative or Poiseuille flow, while the non-dissipative link or Bernoulli flow channel was modeled by a non-linear impedance element. Addition of further coupling links turns the model into a ladder network. For $1 \le m \le 3$ we assert that the circuit behaves as an adding network. By a straightforward extension of Eq. (6), the contingent distribution of voxel pairs having m connecting Bernoulli flow channels with entry and exit orifices displaced by the independent variables $z_1, z_2, z_3 \ldots$ is given by:

$$F'_m(z_1, z_2, \ldots z_m) = K'_m e^{|(z_1+z_2+\ldots z_m)|/\lambda}, \qquad (6)$$

where K'_m is the normalisation constant and λ is the mean pathway between flow channels along the z-axis.

By noting that the flow resistivity element Δk is proportional to z, we can change the variable from z to C by using Eq. (3) and the fact that $z_{m'}/\lambda = \Delta k_{m'}/k_c = C_{m'}/2\zeta$ to obtain an expression equivalent to Eq. (7), namely:

$$F_m(C_1, C_2, \ldots C_m) = K_m e^{-|(C_1+C_2+\ldots C_m)|/2\zeta}, \qquad (7)$$

where we have replaced K'_m by K_m. The quantity k_c introduced in the coordinate transformation is a characteristic flow resistance, for the single Bernoulli flow channel case $\zeta = \langle C\rangle$.

As a generalisation of the connectivity equation, Eq. (3), we write the extended version as:

$$\langle C\rangle_m = \frac{1}{N}\sum_{j,m'} C_{j,m'} = \sum_{j,m'} \left(\frac{\Delta a}{dA}\right)^2 \left(\frac{\Delta k_{j,m'}}{k}\right)/N, \qquad (8)$$

where $1 \le m' \le m$, j refers to the summation over voxels, and m' refers to the summation over m coupling pathways for the j^{th} voxel.

Using the distribution function, Eq. (7), converting Eq. (8) from a discrete to a continuous sum, and taking into account the coordinate transformation from velocity space to connectivity space, we have:

$$\langle C\rangle_m = \int \frac{dC_1}{\sqrt{C_1}} \int \frac{dC_2}{\sqrt{C_2}} \cdots \int \frac{dC_m}{\sqrt{C_m}} \times F_m(C_1, C_2, \ldots C_m) \sum_1^m C_{m'}, \qquad (9)$$

which leads to the connectivity terms $\langle C\rangle_1$, $\langle C\rangle_2$, and $\langle C\rangle_3$ for 1, 2, and 3 Bernoulli pathways, respectively.

RESULTS

In natural porous media such as Bentheimer sandstone the pore size is typically 20 μm. In order to investigate the connectivity variation with slice thickness, it would be necessary in natural materials to have extremely thin slice thicknesses and very high-resolution flow maps. At the present time this is not possible with our equipment. In order to test the theory, therefore, we have constructed model systems comprising glass bead packs with various macroscopic-sized beads ranging from 3–10 mm in diameter. Due to signal-to-noise ratio limitations, the thinnest slice that we are currently able to study is 10 mm. Our initial experiments are, therefore, confined to glass beads of 10-mm diameter.

Fig. 1 shows six velocity-distribution graphs measured using 10-mm glass beads. The continuous curves correspond to the theoretical velocity distribution, Eq. (3), fitted to each experimental distribution using the χ^2

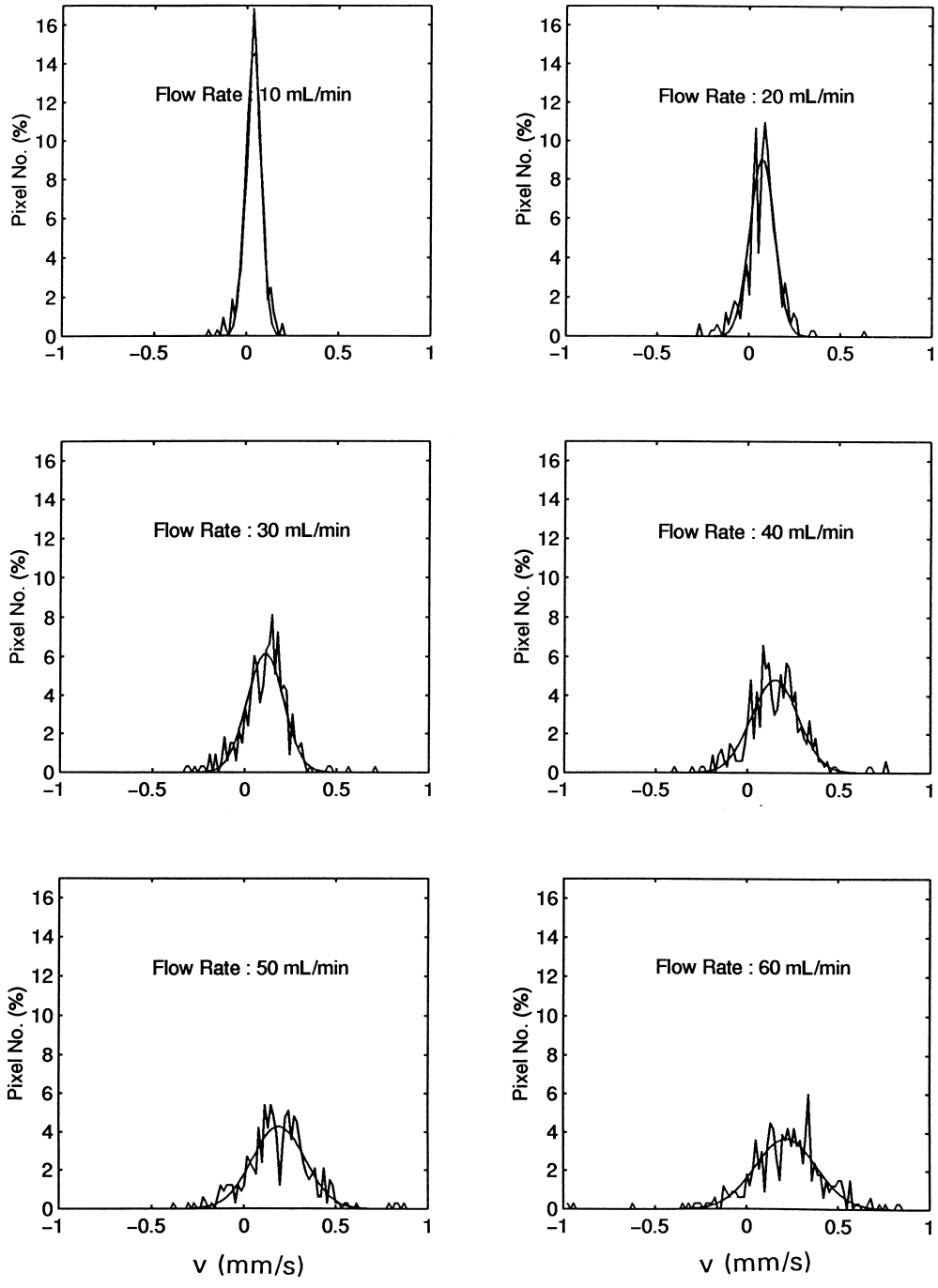

Fig. 1. Graphs of number of pixels having a fluid velocity v (expressed as a percentage) vs. v for the various flow rates indicated. The continuous curves correspond to the Gaussian curve, Eq. (4). The slice thickness $\ell = 30$ mm for all graphs.

test. The mean area under the data curves was used throughout and only a was varied in the fitting process. The mean velocity $\bar{v}$ was taken from the mean value of the data in all cases. As a precursor to this study, we have found that the Mansfield–Issa equation holds true in such model systems. This is demonstrated in Fig. 2, which shows the variance versus $\bar{v}$ for a slice thickness of 40 mm. The variance values were calculated from the raw data. Fig. 3 shows the slope of the variance plot, $\langle C \rangle k/\rho = \langle C' \rangle$ versus the slice thickness ℓ. This shows a considerable variation in $\langle C' \rangle$, which we ascribe to coherence effects.

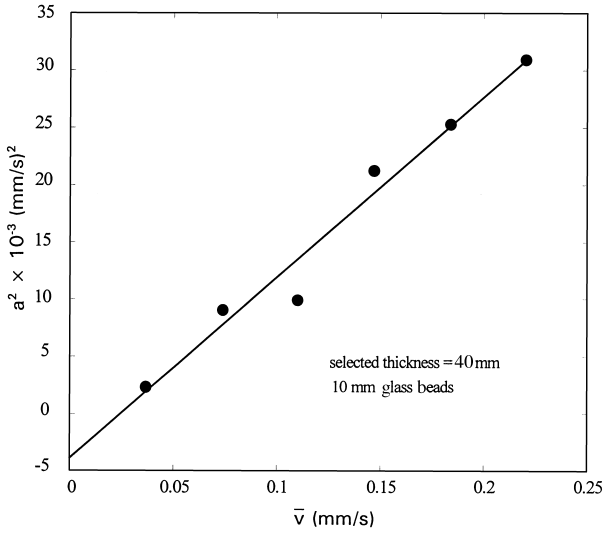

Fig. 2. Graph of a^2 vs. $\bar{v}$ for a glass bead pack comprising 10-mm beads. The slice thickness $\ell = 40$ mm for these data.

Because of the basic periodicity of the bead pack, we assume that for a slice thickness $\ell = 10$ mm equal to the bead diameter, $\langle C' \rangle$ corresponds essentially to $\langle C' \rangle_1$. Similarly for $\ell = 20$ mm there will be on average two beads falling within the slice thickness, so that the connectivity will be dominated essentially by $\langle C' \rangle_2$; likewise for $\langle C' \rangle_3$. From Fig. 3 the connectivity for $\ell = 10$ mm is given by $\langle C' \rangle_1 = 151.8$ μm/s, $\langle C' \rangle_2 = 125$ μm/s, and $\langle C' \rangle_3 = 139.5$ μm/s. Using Eq. (9) and starting with the measured value for $\langle C' \rangle_1$, we find theoretical values of $\langle C' \rangle_2 = 123.6$ μm/s and $\langle C' \rangle_3 = 142.9$ μm/s.

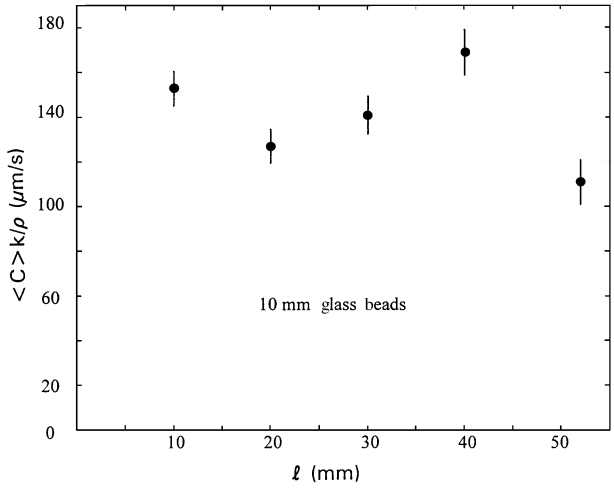

Fig. 3. Graph of $\langle C \rangle k/\rho$ vs. slice thickness ℓ for a glass bead pack comprising 10-mm diameter beads.

For very large slice thicknesses, we expect the initial coherence shown in Fig. 3 to be replaced by a drop in $\langle C' \rangle$, which varies inversely as $\sqrt{\ell}$. Further experimental work is required on 10-mm bead packs in order to substantiate this point.

DISCUSSION AND CONCLUSIONS

The sample container consists of a cylindrical volume with diameter 75 mm and length 150 mm. One of the difficulties with bead packs comprising large diameter beads contained in a finite sample volume is that there are relatively few beads in the statistical assembly. There is, therefore, a clear possibility that the beads will form into regular, close-packed arrays rather than a random arrangement as called for by the theoretical model. Going to a smaller bead size would obviate this difficulty. However, experiments on 5- or 3-mm beads would require a correspondingly thinner slice thickness.

Other concerns are connected with the voxel resolution. We have specifically coarsened the voxel resolution so that it corresponds approximately to the bead diameter. This means that with the 10-mm bead packs, the number of voxels in a given slice is reduced to typically 16×32 voxels. Such small array sizes can call into question the validity of the statistics used in the development of the stochastic theory.

Despite these concerns, the data do seem to agree with most aspects of the theory, in particular the velocity distributions, which are reasonably Gaussian-like in profile, the linearity of the Mansfield–Issa equation, and the expected variation of connectivity with slice thickness.

With the above provisos, we are cautiously optimistic that the model system is behaving as expected. However, it remains to be seen whether these results can be reproduced for smaller bead sizes.

REFERENCES

1. Guilfoyle, D.N.; Mansfield, P.; Packer, K.J. Fluid flow measurement in porous media by echo-planar imaging. J. Magn. Reson. 97:342–358; 1992.
2. Mansfield, P.; Issa, B. Fluid Transport in Porous Rocks. I. EPI Studies and a Stochastic Model of Flow. J. Magn. Reson. A122:137–148; 1996.
3. Mansfield, P.; Issa, B. Fluid transport in porous rocks. II. Hydrodynamic model of flow and intervoxel coupling. J. Magn. Reson. A122:149–156; 1996.